Study of degradation and spatial performance of low Pt-loaded proton exchange membrane fuel cells under exposure to sulfur dioxide in an oxidant stream

Tatyana Reshetenko [a,*], Vincent Laue [b], Ulrike Krewer [b], Kateryna Artyushkova [c]

[a] Hawaii Natural Energy Institute, University of Hawaii, Honolulu, HI, 96822, USA
[b] Institute of Energy and Process Systems Engineering, Technische Universitaet Braunschweig, Franz-Liszt-Straße 35, 38106, Braunschweig, Germany
[c] Department of Chemical and Biological Engineering, University of New Mexico, Albuquerque, NM, 87106, USA

HIGHLIGHTS

- Poisoning effects of SO_2 in air on low-Pt PEMFC were studied with a segmented cell.
- 2 ppm SO_2 caused voltage loss of 240 and 345 mV at 0.2 and 0.8 A cm ^{2}, respectively.
- SO_2 exposure of low-Pt fuel cells at 1.0 A cm ^{2} led to a performance drop below 0.1 V.
- The observed performance is due to S^0 formation at potentials below 0.6 V.
- SO_2 contamination of low-Pt PEMFC led to significant performance drop and degradation.

ARTICLE INFO

Keywords:
PEMFC
Airborne contaminant
SO_2 poisoning
Low-Pt cathode
Segmented cell

ABSTRACT

Sulfur dioxide is a common air pollutant that has an adverse impact on proton exchange membrane fuel cells (PEMFCs). The present study reports the spatial performance and degradation of low-Pt PEMFCs exposed to trace concentrations of SO_2 in a cathode feed stream. PEMFCs exposed to 2 ppm SO_2 resulted in a performance loss of 240 and 345 mV for constant current holds of 0.2 and 0.8 A cm ^{2}. However, the SO_2 contamination of low-Pt fuel cells at 1.0 A cm ^{2} led to a drastic cell potential drop below 0.1 V from the initial 0.605 V and demonstrated that the cathode exposure to SO_2 should be limited to concentrations significantly below 2 ppm for high power operating conditions. The observed voltage and spatial current behavior was attributed to the reduction of SO_2 on Pt to zero-valent sulfur at potentials below 0.6 V. PEMFCs recovered performance only after potential cycling, insuring the oxidation of the formed S^0 species at potentials higher than 0.8 V. A comparison of the electrochemical parameters before and after PEMFC poisoning revealed a substantial decrease in electrochemical surface area of up to 45.2% and a final performance loss of 60–100 mV.

1. Introduction

Proton exchange membrane fuel cell (PEMFC) technology is making rapid progress due to an emerging commercialization for automotive and stationary applications as well as a developing hydrogen infrastructure. To overcome existing techno-economic restrictions of fuel cell technology and facilitate market penetration, the next generation of PEMFCs requires a substantial reduction in the cost of their production, which can be achieved through economy of scales and by decreasing platinum content in the electrodes. At the same time, the performance, durability and reliability of low-Pt fuel cells should be the same or comparable to high-Pt PEMFCs. Currently, significant progress has been made in reducing Pt loading [1]. The factors that affect and determine fuel cell performance and degradation are carbon corrosion, platinum nanoparticle migration and agglomeration, electrochemical Ostwald ripening and platinum redeposition on polymeric matrixes or on another Pt nanoparticle [2]. It should be noted that all these factors are more pronounced and play a significant role in decreasing the performance and durability of low-Pt electrodes and thus, they increase the degradation rate [3–6].

Most fuel cells operate with air as an abundant and free of charge oxidant. However, ambient air typically contains a variety of inorganic

* Corresponding author.
E-mail address: tatyanar@hawaii.edu (T. Reshetenko).

and organic pollutants as well as particulates originating from natural and anthropogenic emission sources. All of these airborne contaminants compromise the performance of commercial high-Pt membrane electrode assemblies (MEAs), as shown in previous publications [7–21]. Among these impurities, SO_2 is of special interest due to its high concentration in urban air (from 5 to 20 ppb to several ppm) [22–24] and its strong and irreversible effects on PEMFCs [7,8,25–40]. The extent of cathode poisoning by SO_2 strongly depends on the operating voltage since various electrochemical reactions involving adsorbed sulfur-containing species can occur at different cathode potentials [41, 42]. Studies using a rotating ring-disk electrode technique, a cyclic voltammetry coupled with Fourier transformed infrared (FTIR) spectroscopy, X-ray photoelectron spectroscopy (XPS) and an X-ray absorption near edge structure (XANES) analysis shows that SO_2 adsorption on Pt results in the formation of elemental sulfur at 0.5 V, a mixture of various adsorbed SO_2 species and bisulfate (HSO_4^-) ions are generated at 0.6–0.8 V, while SO_4^{2-} is produced at potentials of 0.9 V and higher [41–52].

The performance of PEMFCs with a Pt loading of 0.4 mg_{Pt} cm^{-2} for both the anode and cathode in the presence of several ppm of SO_2 in the air stream is shown to be dramatically affected. For example, voltage loss is found to be in the range of 200–300 mV in a high power operation, and only partial recovery was reported when SO_2 introduction in the cathode stream is stopped [20,25,26,40,53] due to strongly adsorbed SO_x species and elemental sulfur formation on the Pt surface [41, 43–45]. Only special cathode treatments, such as potential cycling or multiple measurements of polarization curves, can restore the fuel cell performance, oxidizing the sulfur-containing species to soluble sulfates and bisulfates, which facilitates their removal. However, a performance loss after the recovery procedure was detected and was shown to be 20–50 mV [32,53]. The current 2020 US DOE technical target regarding electrocatalysts for transportation applications requires 0.125 mg_{Pt} cm^{-2} for both electrodes [54]. Due to this trend in reducing Pt loading, it is very important to understand the environmental adaptability and tolerance of low-Pt fuel cells to the main air impurities and establish air quality requirements.

The current work is a continuation of our previous publications on the effects of various airborne contaminants on spatial PEMFC performance [10–14,53] and presents thorough studies of spatial low-Pt PEMFC behavior under cathode exposure to SO_2. It should be noted that the majority of the available in the literature data on the evaluation of PEMFC behavior in the presence of fuel or air pollutants was performed using a single cell approach, which provided only average values of current and voltage for the active area of an MEA. On the other hand, segmented cell systems reveal localized electrochemical parameters, such as voltage, current and impedance, and are widely used to study local inhomogeneities occurring during fuel cell operation under different operating and environmental conditions. To understand the interplay between localized performance during poisoning and the degradation of low-Pt MEAs, a segmented cell system developed at Hawaii Natural Energy Institute (HNEI) was employed [55]. The obtained results on the distribution of localized main electrochemical parameters, such as current, voltage and impedance, provide unique and beneficial information on processes occurring in active areas of an MEA and offer tremendous opportunities for future modeling efforts.

2. Experimental

All experimental tests were performed using a fuel cell test station and a segmented cell system developed at HNEI. The segmented cell setup consists of cell hardware, a custom-designed current transducer system, a data acquisition device and a single cell test station (Fig. 1a and b). We operated the segmented cell system as a single cell and controlled only overall cell current or voltage using the test station and applying standard testing protocols. Such procedure mimics conditions relevant to real fuel cell operation. The segmented cell hardware is built

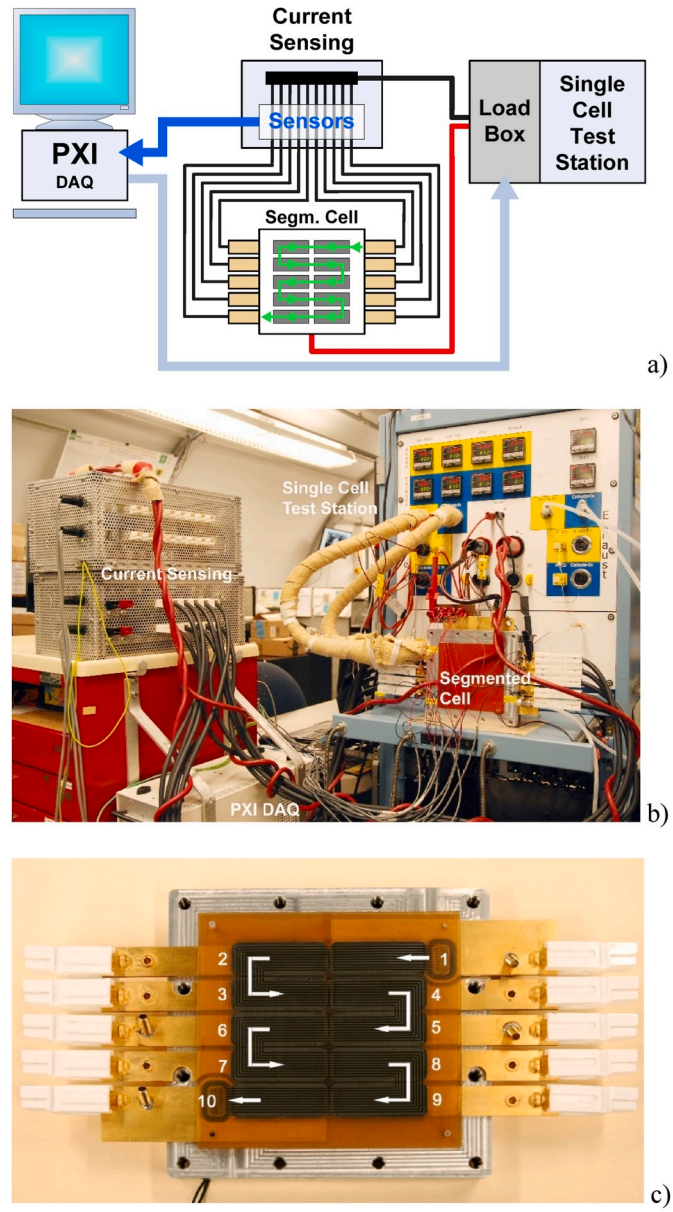

Fig. 1. Schematic of the segmented cell system (a), overall view of the tests station and the segmented cell (b) and segmented flow field (c). Fig. 1 a) is reprinted from Ref. [55] T.V. Reshetenko, G. Bender, K. Bethune, R. Rocheleau, Electrochim. Acta 56 (2011) 8700.

based on a 100 cm^2 cell and consists of non-segmented and segmented flow field plates. The segmented flow field plate was applied to the cathode and has 10 segments with an area of 7.6 cm^2 connected in sequential order from segment 1 (cell inlet) to segment 10 (cell outlet) (Fig. 1 c). Each segment has its own separate gas diffusion layer (GDL) and current collector. It should be also noted that both flow field plates have the same ten parallel channel serpentine design and arranged in co-flow configuration. The segmented cell system and hardware were described in details in our previous publication [55].

We used commercially available non-segmented 100 cm^2 MEAs manufactured by Gore for the SO_2 contamination tests. The Pt/C catalyst loading was 0.1 mg_{Pt} cm^{-2} for the anode and cathode and Sigracet 25 BC was applied as GDLs. The gasket material for both electrodes was made of Teflon with thicknesses of 125 μm.

The SO_2 poisoning experiments were performed using H_2/air at a 2/2 stoichiometry, 100/50% relative humidity, 150/150 kPa backpressure and 80 °C. The contamination tests were done by injection of a dry

mixture of 75 ppm SO_2 in air into the main stream of humidified air to the cathode. The desired SO_2 concentration entering the cathode was set by adjusting the flow rate of the injected dry mixture of SO_2 and air. In our work, final SO_2 content was 2 ppm for all tests. The specified cathode humidification was maintained by increasing the temperature of the humidifier unit to compensate for the dry contaminant stream. The MEAs were operated under control of the whole cell current at 0.2, 0.8 and 1.0 A cm^{-2}. The polarization curves (VI curves) were recorded at the same operating conditions as the poisoning tests with the H_2/air as well as H_2/He + O_2 (21 vol%) and H_2/O_2 to determine the activation, ohmic and mass transfer (permeability and diffusion) losses, as reported in Refs. [55,56].

Spatial electrochemical impedance spectroscopy (EIS) characterizations were conducted simultaneously for each segment as well as for the overall cell during the VI and SO_2 poisoning tests. The frequency range was from 0.05 Hz to 10000 Hz and measurements were performed with 11 steps/decade. The perturbation signal did not exceed of 10 mV. The electrochemical surface area (ECSA) was determined by cyclic voltammetry (CV) using Solartron SI 1287/electrochemical interface. CV was performed over a potential range from 0.1 to 1.2 V vs. the reversible hydrogen electrode at a scan rate of 20 mV s^{-1}. To restore the cathode ECSA after SO_2 poisoning, we applied 13 scans from 0.1 to 1.2 V and additional 3 scans with an extended upper potential of 1.5 V.

Anode and cathode catalysts were investigated by transmission electron microscopy (TEM) using a Hitachi HT-7700 instrument. The catalyst surfaces from both electrodes and GDLs was evaluated by X-ray photoelectron spectroscopy (XPS). High-resolution F 1s, C 1s, O 1s, Pt 4f and S 2p spectra were obtained by Kratos XPS ultra DLD spectrometer operating with an Al Kα monochromatic source at 225 W.

3. Results and discussion

3.1. Spatial performance of low-Pt PEMFC under SO_2 exposure

Fig. 2 presents the profiles of individual segment voltage and normalized current densities under 2 ppm SO_2 exposure at overall cell currents of 0.2, 0.8 and 1.0 A cm^{-2}. The normalized current density is a proportion between the measured current density and its initial value, which was obtained before contamination. All contamination tests were done using air as a cathode feed gas. For comparison purposes, we performed a reference test at the same operating conditions as the poisoning experiments, at a constant current of 0.8 A cm^{-2} for 120 h (Fig. 2 d). All contamination tests include several stages: 1) pre-poisoning, 2) poisoning and 3) self-recovery. The pre-poisoning stage

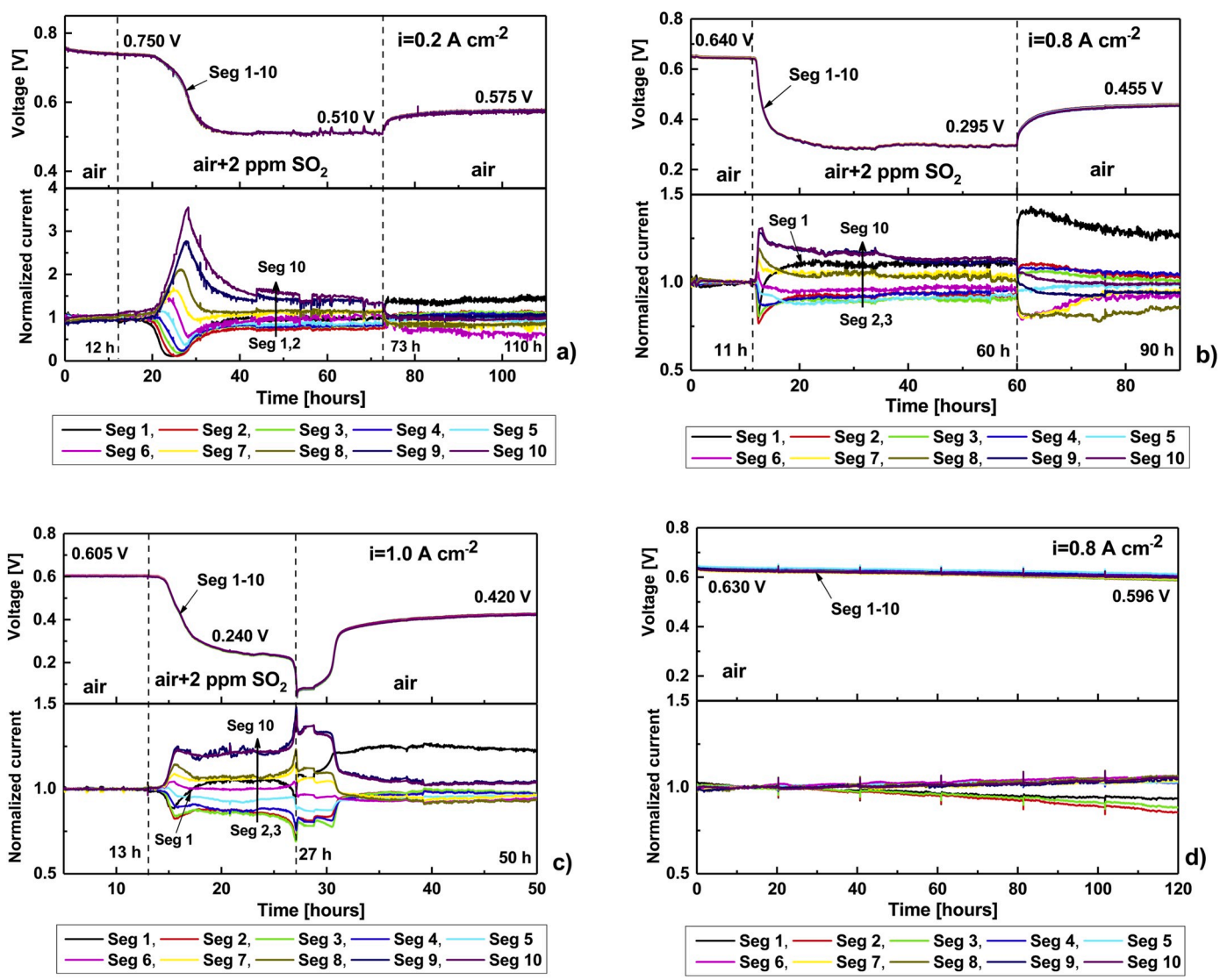

Fig. 2. Profiles of voltage and normalized current densities vs. time under 2 ppm SO_2 poisoning at overall current density of 0.2 (a), 0.8 (b), 1.0 A cm^{-2} (c) and a reference test without SO_2 contamination at 0.8 A cm^{-2} (d). Anode/cathode: H_2/air, 2/2 stoichiometry, 100/50% RH, 150/150 kPa, 80 °C.

was carried out using pure air as the cathode feed for 11–13 h to determine the initial fuel cell performance. Average cell voltages of 0.750, 0.640 and 0.605 V were obtained at 0.2, 0.8 and 1.0 A cm^{-2}, respectively (Fig. 2a–c). The initial distribution of the localized current densities was found to be in the range from 0.15 to 0.24 A cm^{-2} at 0.2 A cm^{-2} of the overall cell current, whereas at 0.8 A cm^{-2}, the individual segment current densities varied from 0.7 to 0.89 A cm^{-2}. A further increase to 1.0 A cm^{-2} in the cell operating current led to a current distribution from 0.81 to 1.17 A cm^{-2}. In all cases, the produced current density of the inlet segments 1–3 was higher than that of the outlet segments 9 and 10.

The introduction of 2 ppm SO_2 in the cathode feed stream led to a decrease in the cell and segment voltages as well as caused localized current redistribution. The performance loss at a steady state was 240 and 345 mV for constant current holds of 0.2 and 0.8 A cm^{-2} (Fig. 2a and b), respectively. The obtained performance is in good agreement with those of previously published results [25–27,33,36,53]. Completely different behavior was detected during SO_2 exposure at 1.0 A cm^{-2}, which caused a voltage drop from 0.605 V to 0.240 V and a further drastic voltage decrease below 0.1 V (Fig. 2 c). A similar performance drop below 0.1 V was reported by S. Tsushima et al. [36] for fuel cells exposed to high SO_2 concentrations of 100–250 ppm and varied relative gas humidities. As soon as the cell voltage dropped below 0.1 V, the SO_2 injection was stopped, resulting in an overall PEMFC exposure of 14 h, while the durations of the poisoning stage were 61 and 49 h for the 0.2 and 0.8 A cm^{-2} tests. Interestingly, we also noted a delay of 7 h for the cell response at low current density operation (Fig. 2 a). A similar observation was also found for high-Pt PEMFCs exposed to SO_2 at 0.2 A

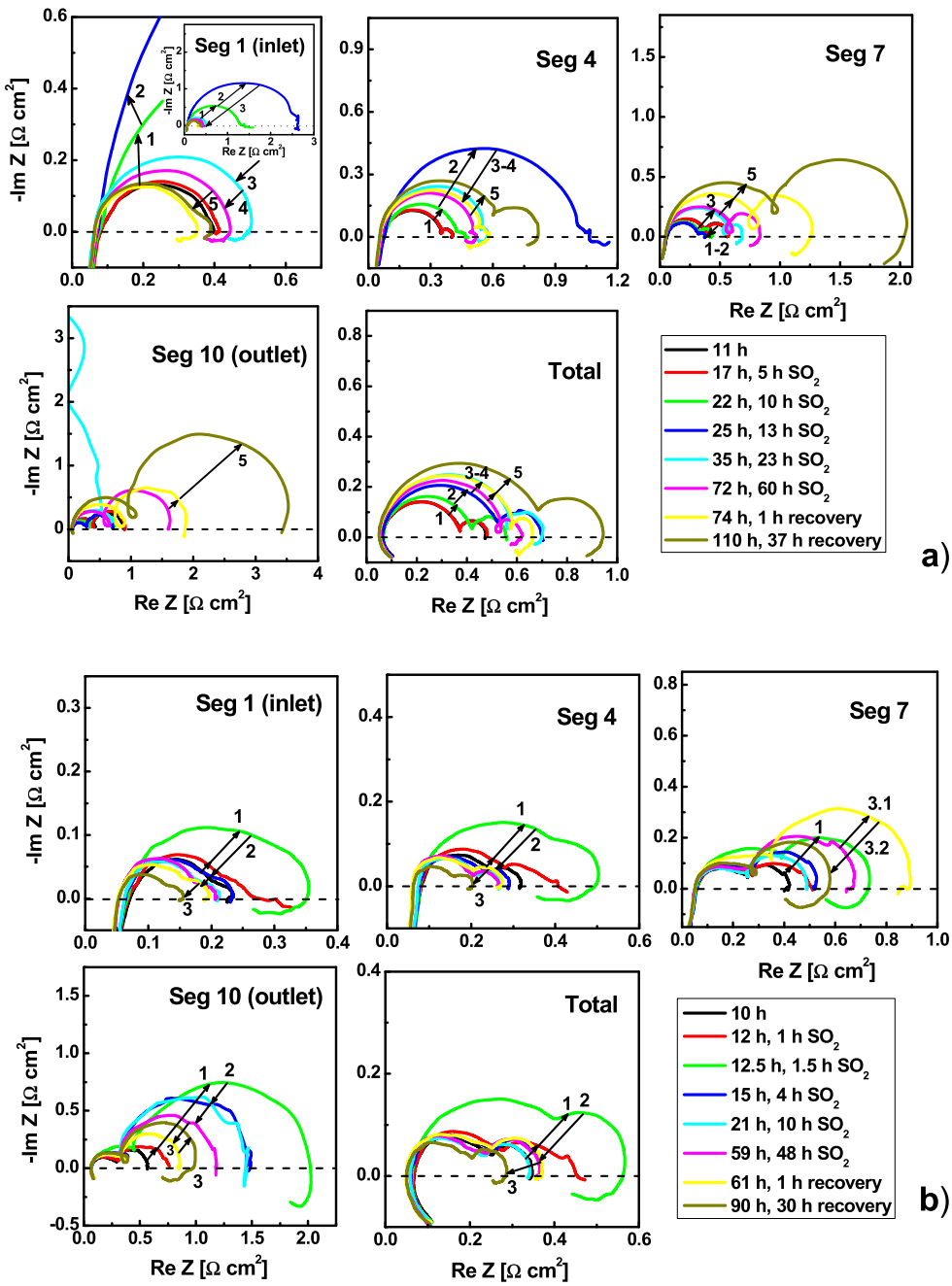

Fig. 3. EIS for segments 1, 4, 7, 10 and the total cell during SO_2 contamination at an overall current density of 0.2 (a), 0.8 (b), 1.0 A cm^{-2} (c) and a reference test without SO_2 poisoning at 0.8 A cm^{-2} (d). Anode/cathode: H_2/air, 2/2 stoichiometry, 100/50% RH, 150/150 kPa, 80 °C.

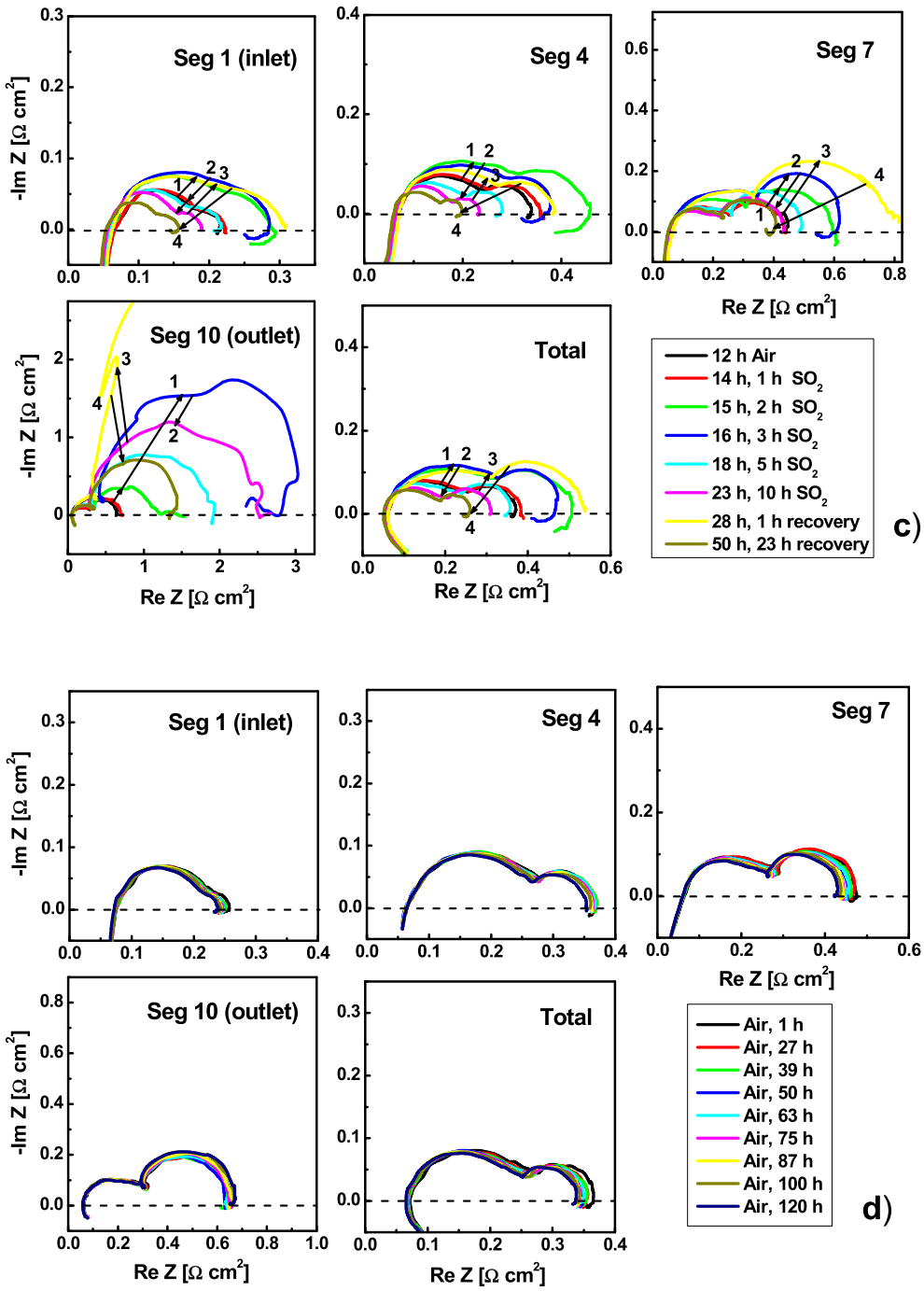

Fig. 3. (*continued*).

cm^{-2} [53]. This finding could be attributed to the slow adsorption of SO_x species on the Pt surface at potentials of 0.7–0.75 V, until SO_x coverage reached a critical value; afterwards SO_2 affected the cell voltage, causing its decrease to a point that the adsorbed SO_x was reduced to zero-valent sulfur. A slight delay was also detected for the case of 1.0 A cm^{-2} (Fig. 2 b), which could originate from a possible dilution of SO_2 in water that was produced at the cathode, thus, postponing the cell response.

In all tests, the localized current density distribution went through a similar pattern. At the beginning of the poisoning stage, the current densities of inlet segments 1–5 went down, while outlet segments 6–10 generated higher currents. As soon as the segment currents reached their extremum values, we observed a reverse of spatial performance when the current production from the outlet segments decreased, but at the same time, there was an increase in current densities for the inlet of MEAs. The extremum values of the individual currents agreed with an inflection point of the voltage profiles at 0.590, 0.520 and 0.490 V for 0.2, 0.8 and 1.0 A cm^{-2}, respectively. Similar localized current behavior was previously detected and described for SO_2 and CH_3CN cathode poisoning of high-Pt PEMFCs and was attributed to electrochemical reduction of sulfur-containing species on Pt [11,53].

At the self-recovery stage, the cathode was fed by pure air, and the cell and individual segments gained only a partial recovery. The cell

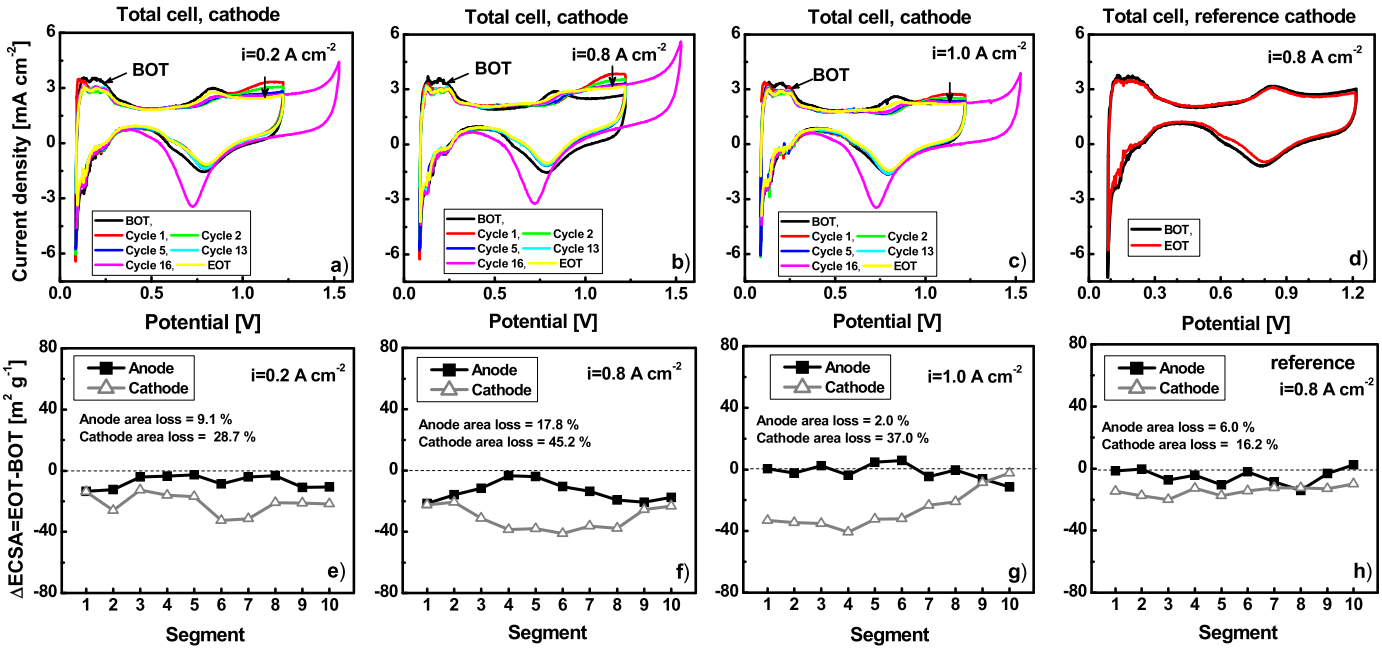

Fig. 4. CV recorded for the overall cathode after SO_2 poisoning at 0.2 (a), 0.8 (b), 1.0 A cm ^{2} (c) and a reference test at 0.8 A cm ^{2} (d). Distributions of anode and cathode ECSA differences at 0.2 (e), 0.8 (f), 1.0 A cm ^{2} (g) and a reference run at 0.8 A cm ^{2} (h). Anode/cathode: H_2/N_2, 0.75/0.75 l min ^{1}, 100/100% RH, 35 °C, ambient pressure, 20 mV s ^{1}.

voltage was found to be 0.575 V (vs. the initial 0.705 V), 0.455 V (vs. the initial 0.640 V) and 0.420 V (vs. the initial 0.605 V) for 0.2, 0.8 and 1.0 A cm^{-2}, respectively. The lack of full recovery is attributed to the formation of S^0 and strongly adsorbed sulfur-containing species on the Pt surface, as shown in our previous work [53]. At the same time, the reference sample showed a slight decay in performance under a constant current hold at 0.8 A cm^{-2}; the voltage loss was found to be 30–35 mV, and the performance of segments 1-3 decreased by 8–12% (Fig. 2 d).

Localized impedance spectra for selected segments the and overall cell are shown in Fig. 3. Initial impedance curves were measured in pure air before SO_2 injection. These spectra typically consisted of high-frequency semicircle (1000–10 Hz) due to cathode charge transfer resistance and double layer capacitance for the oxygen reduction reaction and low-frequency arc (1–0.1 Hz) accounted for the diffusion processes at the cathode [57]. A growth in the low-frequency arc diameter is observed from the segment 1 to segment 10 due to oxygen depletion and water accumulation downstream.

The effects of cathode exposure to SO_2 at 0.2 A cm^{-2} was not detected by EIS after 5 h of poisoning (Fig. 3 a). However, 10 h of contamination resulted in an increase in the charge transfer resistances of segments 1–4; other segments did not reveal any changes (Fig. 3 a, pathway 1). A further increase in the impedance response for the inlet of MEA continued with SO_2 introduction to the air stream (Fig. 3 a, pathway 2). A reverse trend in local EIS behavior was observed after ~20 h of cathode poisoning: the impedance response of segments 1-4 decreased, while segments 7–10 showed an increase in charge transfer and mass transfer resistances (Fig. 3 a, pathways 3–4). This observation was in good correlation with the spatial voltage and current distributions (Fig. 2 a) and the inflection point at the voltage profile (~0.590 V) corresponded to the changes in local currents and impedance. EIS curves recorded during self-recovery clearly showed that only segment 1 recovered its performance, while others were characterized by increased charge and mass transfer resistances (Fig. 3 a, pathway 5). It should also be noted that we observed a low-frequency pseudo-inductance starting after ~20 h of SO_2 exposure as well as during self-recovery.

An increase in operating current density to 0.8 A cm^{-2} led to a trend resembling the observed one at the low current operation; however, there are some details and differences that should be emphasized (Fig. 3 b). First, the cathode exposure to SO_2 within 1 h caused an immediate increase in EIS response for all segments; this correlates to the effect visible in the voltage level (Fig. 2 b). Moreover, we detected a drift of the impedance values at low frequency, indicating changes in the impedance of the segments during the measurement because recording EIS at the low frequency required a finite time. Similar EIS features were found in the case of CO anode poisoning and were previously discussed in Refs. [58,59]. PEMFC poisoning for 1.5 h corresponded to the inflection point of the voltage profiles (~0.520 V) as well as the extremum values of the segment current densities (Fig. 2 b) and resulted in a further increase in charge and mass transfer resistances for the entire cell and an appearance of low-frequency pseudo-inductance (Fig. 3 b, pathway 1). A low-frequency inductance meant that there is a phase delay in current signal followed a perturbation because of slow relaxation of adsorbate coverage compared to the oxygen reduction. In addition, a low frequency inductance indicated on successive electron transfer reactions of adsorbed contaminant species occurring with the formation of

Table 1
Anode and cathode ECSA before and after SO_2 exposure tests.

Operating conditions	Anode ECSA [m^2 g ^{1}]		Cathode ECSA [m^2 g ^{1}]		ΔECSA [%]		Tafel slope [mV/dec]	
	BOT	EOT	BOT	EOT	anode	cathode	BOT	EOT
0.2 A cm ^{2}	80.5	73.2	74.3	53.0	9.1	28.7	71	75
0.8 A cm ^{2}	77.9	64.0	69.7	38.2	17.8	45.2	63	76
1.0 A cm ^{2}	81.2	79.7	71.2	44.9	2.0	37.0	74	72
Reference	82.5	77.6	89.5	75.0	6.0	16.2	73	73

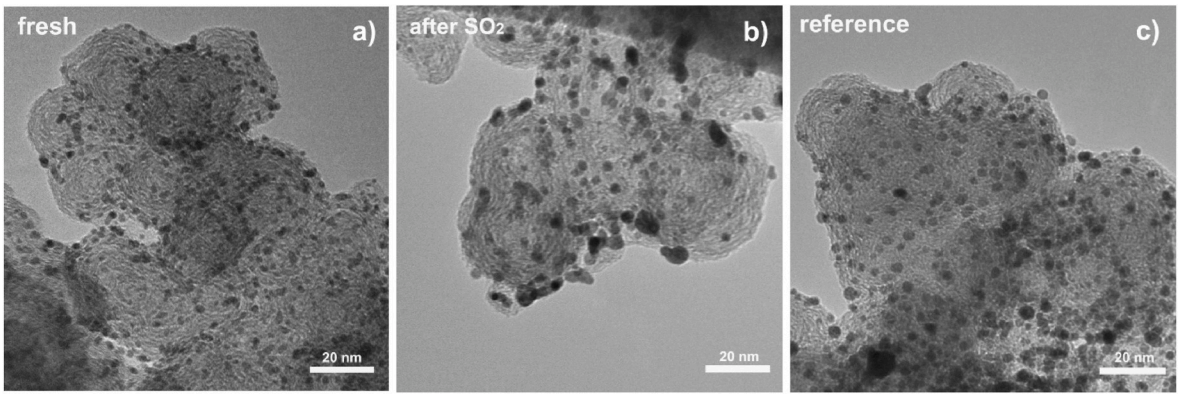

Fig. 5. TEM photos of the cathode Pt/C catalyst: fresh (a), after SO_2 contamination at 0.8 A cm ^{2} (b) and after the reference test at 0.8 A cm ^{2} (c).

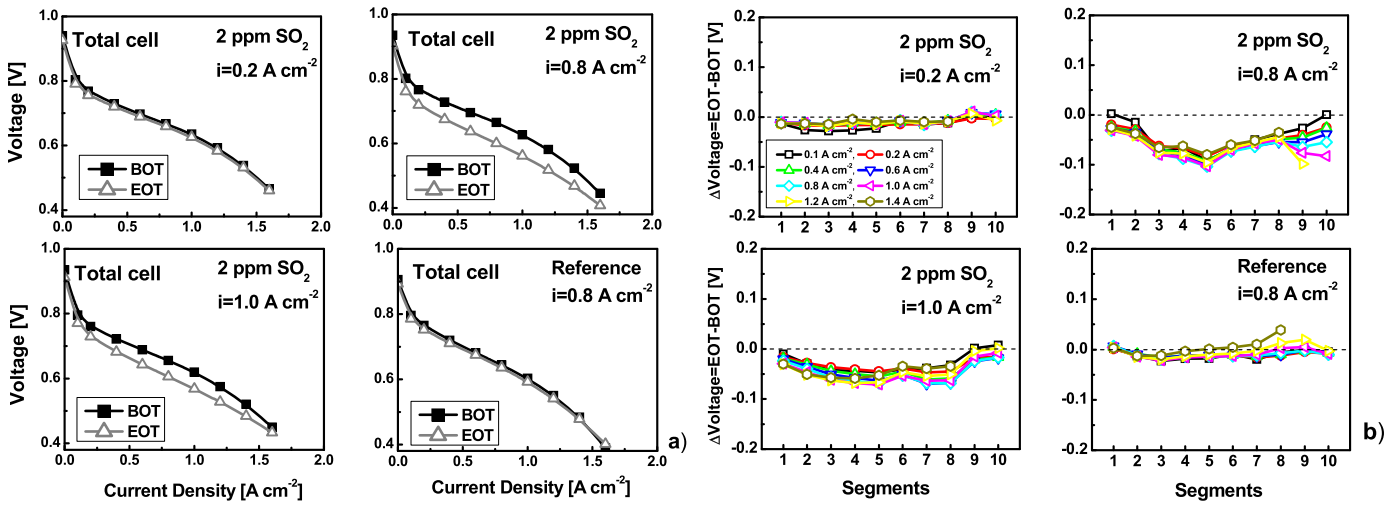

Fig. 6. A comparison of BOT and EOT polarization curves for the total cell (a) and distributions of performance differences between EOT and BOT for different operating current holds (b). Anode/cathode: H_2/air, 2/2 stoichiometry, 100/50% RH, 150/150 kPa, 80 °C.

intermediates on the Pt surface [60–64]. A similar pseudo-inductive feature was detected during anode exposure to CO and cathode poisoning by C_2H_2, CH_3CN, CH_3Br and naphthalene at potentials at which electrooxidation of CO and electroreduction of air contaminants can take place in parallel with those of hydrogen oxidation and oxygen reduction, respectively [10–12,14,59,65]. The detection of the pseudo-inductance clearly indicated the electroreduction of sulfur-containing species at a potential of ~0.520 V. Furthermore, SO_2 exposure decreased the impedance of the segments, and the low-frequency inductance disappeared (Fig. 3 b, pathway 2). After the cathode contamination, an operation with pure air led to a reduction in impedance response for all segments and the formation of low-frequency inductance after 30 h of self-recovery (Fig. 3 b, pathways 3), similar to that of the low current case (Fig. 3 a, pathways 5). It should be noted that during poisoning, the outlet segments showed some noise at low frequency range which could be explained by altered water management, since these segments produced greater current than others (Fig. 2) and flooding effects are expected.

Spatial EIS of PEMFC operated at a constant current hold of 1.0 A cm^{-2} revealed that 1 h of SO_2 poisoning did not significantly impact the impedance of the cell (Fig. 3 c). However, exposure to the contaminant within 2–3 h showed an increase in charge and mass transfer resistances and the formation of low-frequency inductances similar to that at 0.8 A cm^{-2} (Fig. 3 c, pathway 1). Interestingly, the outlet segments 9 and 10 demonstrated that steady state conditions were not reached at 2 h of poisoning, and it was possible to see a drift in the impedance response in the low-frequency range. Injection of SO_2 for 5–10 h resulted in a decrease of the EIS for all segments (Fig. 3 c, pathway 2). The initial stage of recovery after 1 h in pure air is characterized by an increase in impedance for the entire cell compared to that of the poisoned cell for 10 h (Fig. 3 c, pathway 3), but 23 h of self-recovery partially restored the segment impedance; although the EIS response of the inlet segments is smaller than the initial values, while outlet segments 9 and 10 have greater impedance values compared to that of the non-poisoned state (Fig. 3 c, pathway 4). The reference test clearly showed that the spatial EIS of the PEMFC operated with pure air at a constant current hold of 0.8 A cm^{-2} for 120 h only slightly varied (Fig. 3 d).

3.2. *Effects of SO_2 on ECSA and fuel cell performance before and after poisoning*

Successive CV cathode scans measured in the H_2/N_2 gas configuration at 35 °C after SO_2 poisoning are shown for the constant current operation at 0.2, 0.8 and 1.0 A cm^{-2} in Fig. 4a–c), respectively. The features of these three sets of CVs are similar to each other and have been described in our previous paper [53]. On the first scan (0.1 V → 1.2 V), a significant suppression of the hydrogen region was observed due to blocking of the Pt surface by zero-valent sulfur (S^0_x) species originating from SO_2 electroreduction. It should be noted that the ECSA loss determined from the first CV scan was found to be in the range of 45–65%. In addition, a pronounced positive shift was detected for the formation of Pt oxides as well as the appearance of a broad peak at 1.12

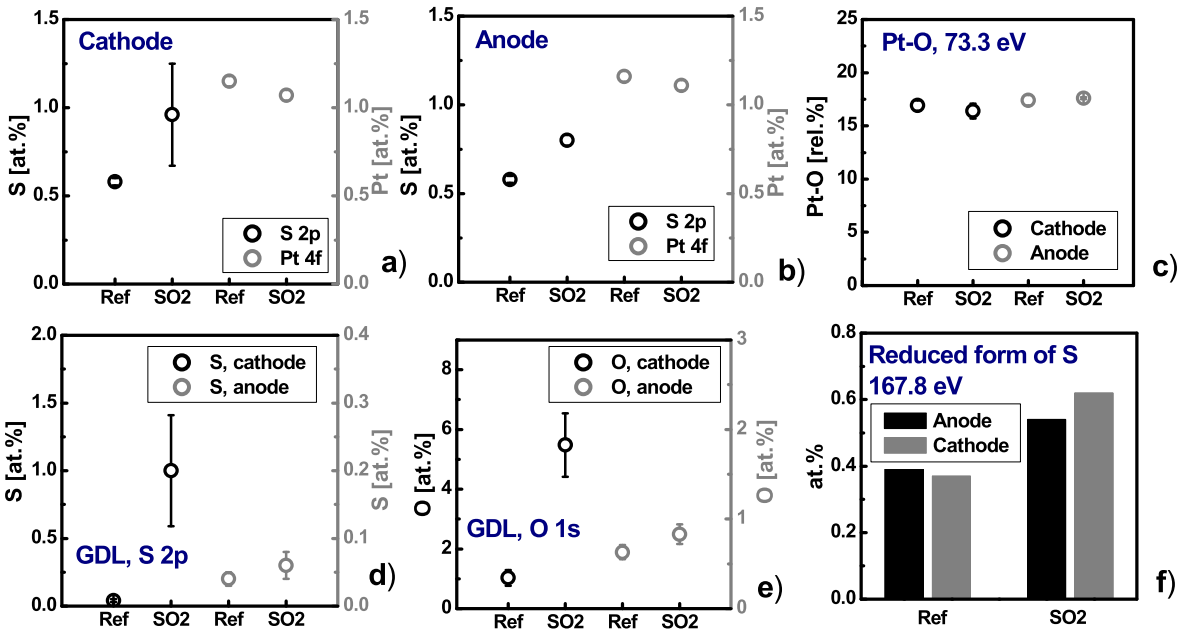

Fig. 7. Surface concentration of S and Pt for the reference and the exposed cathode (a) and anode (b); the relative amount of Pt–O detected for the reference and the SO_2 contaminated sample (c); surface concentration of S 2p (d) and O 1s (e) for the reference and the anodic and cathodic GDLs; surface concentration of reduced forms of S on the reference and poisoned MEA (f).

Table 2
Surface atomic concentration for the fresh MEA, reference sample, SO_2 exposed electrodes and GDLs at 0.8 A cm ^{2} based on the average values from XPS measurements of segments 1, 5 and 10.

Sample	Surface atomic concentration [at.%]								
	C 1s	F 1s	O 1s	S 2p	Pt 4f	S/F	S elem/S–C 164.0 eV	SO_3 167.8 eV	SO_4 169.2 eV
Fresh MEA, anode	43.5	48.2	6.4	0.69	1.23	0.014	0.03	0.43	0.24
Reference, anode	47.0	45.1	6.1	0.58	1.16	0.013	0.02	0.49	0.17
Exposed to SO_2, anode	45.1	45.9	7.1	0.80	1.11	0.017	0.03	0.54	0.23
Fresh MEA, cathode	44.2	47.0	6.7	0.83	1.25	0.018	0.04	0.60	0.19
Reference, cathode	47.4	44.5	6.4	0.58	1.15	0.013	0.02	0.37	0.19
Exposed to SO_2, cathode	46.3	44.2	7.5	0.96	1.07	0.022	0.05	0.62	0.29
Reference, anode GDL	60.3	39	0.63	0.04	0.01				
Exposed to SO_2, anode GDL	62.0	37.1	0.83	0.06	–				
Reference, cathode GDL	59.5	39.4	1.03	0.04	0.01				
Exposed to SO_2, cathode GDL	58.1	35.4	5.48	1.00	–		0.61	0.38	0.01

Table 3
Relative concentration of surface species for fresh, reference and SO_2 exposed electrodes from XPS measurements.

Sample	Relative concentrations [rel.%]					
	S elem/ S–C 164.0 eV	SO_3 167.8 eV	SO_4 169.2 eV	Pt 71.4 eV	Pt–C 72.2 eV	PtO 73.3 eV
Fresh MEA, anode	3.9	61.7	34.4	34.8	42.9	22.3
Reference, anode	3.5	66.4	30.1	41.4	41.2	17.4
Exposed to SO_2, anode	3.7	66.7	29.6	41.9	40.5	17.6
Fresh MEA, cathode	4.3	72.4	23.3	35.1	42.4	22.5
Reference, cathode	4.1	63.5	32.3	42.5	40.6	16.9
Exposed to SO_2, cathode	4.8	65.2	30.0	42.9	40.6	16.4

V due to electrooxidation of adsorbed S^0_x species to water-soluble sulfate SO_4^{2-}, as proposed by Loučka and Contactor [43–45]. Sulfates and bisulfates desorbed from the Pt surface at potentials greater than 1.1 V [66], and this resulted in a cleaning of the Pt surface, making it available for hydrogen/oxygen adsorption in the next cycle. Indeed, the second scan demonstrated a partial recovery in hydrogen desorption/adsorption regions as well as a reduction in the sulfur oxidation peak.

This peak was less pronounced for the cell operated at 1.0 A cm^{-2} (Fig. 4 c), which could be explained by the fact that the cathode was poisoned by SO_2 for only 14 h, while for other constant current holds, the cells were exposed for much longer time periods. Three additional scans with an extended upper potential of 1.5 V were carried out to ensure the removal of sulfur-containing species after the initial thirteen CV cycles from 0.1 to 1.2 V. Despite the applied potential cycling, some residual sulfur species remained on the Pt surface because a 30 mV positive shift in Pt oxidation was observed after all the CV cycling was completed.

Fig. 4e–g) present distributions of the anode and cathode ECSA

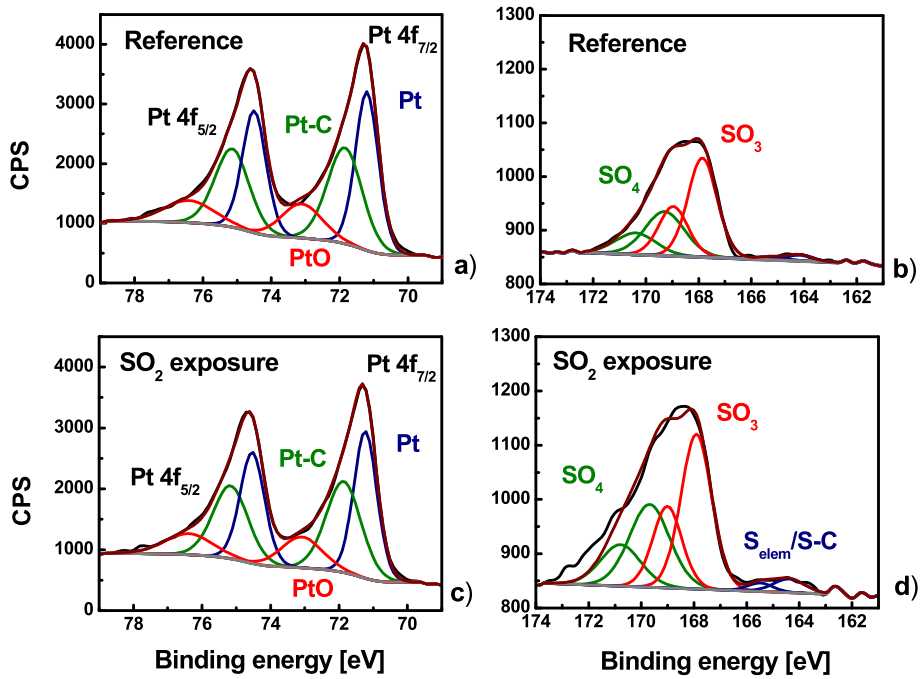

Fig. 8. High-resolution XPS spectra of Pt 4f and S 2p for the reference cathode and segment 1 of the cathode after SO_2 exposure tests.

differences between the end of test or after the SO_2 exposure (EOT) and beginning of the test (BOT). PEMFC exposure to SO_2 at the low current caused a relatively uniform decrease in cathode and anode ECSA along the MEA active area compared to that of the high current operating conditions. Analysis of the spatial cathode ECSA revealed that the greatest ECSA drop was found for segments 3–8 at 0.8 A cm^{-2}, whereas the Pt surface area loss gradually decreased from the inlet to the outlet at 1.0 A cm^{-2} (Fig. 4f and g). The anode ECSA was seriously affected only in the case of 0.8 A cm^{-2}. Fig. 4 d) and h) present the cathode CVs and ECSA distributions for the reference sample. The ESCA data are summarized in Table 1 and show that the Pt cathode ECSA loss under 2 ppm SO_2 exposure was 28.7, 45.2 and 37% at 0.2, 0.8 and 1.0 A cm^{-2}, respectively, while the reference sample showed a cathode ECSA drop of 16.2%.

These results are strongly supported by TEM studies of the anode and cathode catalysts after SO_2 contamination (Fig. 5). The Pt particle sizes from the anode and cathode in fresh MEA were found to be in the range of 2.0–2.5 nm (Fig. 5 a). The cathode exposure to SO_2 led to a growth of Pt particles to 3–10 nm with detection of agglomerates containing a diameter greater than 10 nm and formed a broad particle size distribution (Fig. 5 b). A comparison of the cathode exposed to SO_2 and the reference showed that SO_2 accelerated Ostwald ripening and particles agglomeration (Fig. 5 b) and c)). TEM evaluation of cathode catalysts from segment 1, 5 and 10 after SO_2 poisoning did not show any significant effect of location on particle size. The size of Pt particles at the anode varied in a narrow range from 2 to 5 nm. At the same time, the reference cathode and anode demonstrated moderate increase in particle size in the range of 2–4 nm (Fig. 5 c).

The polarization curves measured for the total cells of the samples before and after SO_2 poisoning are presented in Fig. 6 a). It should be noted that the VI curves were recorded after the CV recovery procedure. A comparison of the BOT and EOT polarization curves showed that even after potential cycling, there is a significant performance drop of up to 70–80 mV caused by SO_2 exposure at high current density operation (0.8–1.0 A cm^{-2}); this may be correlated to Pt particle growth. Cathode poisoning by SO_2 at 0.2 A cm^{-2} resulted in a performance loss of 20–30 mV, while the reference test revealed a voltage drop no greater than 15 mV. The impact of SO_2 on spatial performance in terms of the distribution of voltage differences between the EOT and BOT at fixed current densities and as functions of segment locations is shown in Fig. 6 b). The data in Fig. 6a) and b) are complimentary to each other and clearly demonstrate that operation with pure air and SO_2 contamination at low current led to a uniform voltage loss distribution downstream, while high current operation (0.8–1.0 A cm^{-2}) caused non-homogeneous performance as well as degradation with local performance loss of up to 100 mV. The obtained data in Fig. 6 b) revealed that segments 3–8 seem to be affected by SO_2 exposure the most and exhibit the highest performance drop compared to inlet segments 1 and 2. Interestingly, the performance of segments 9 and 10 after poisoning at 0.8 A cm^{-2} showed a significant voltage loss depending on the current density, while for the case of 1.0 A cm^{-2}, these outlet segments almost fully recovered their initial performance. Furthermore, the distribution profiles of voltage differences in Fig. 6 b) were in good agreement with that of the distribution profiles of cathode ECSA differences (Fig. 4e–h), which indicated a strong correlation between ECSA and performance.

The BOT and EOT performances were analyzed in terms of activation, ohmic and mass transfer losses to determine the origin of the voltage decrease [55]. The results revealed that the observed voltage losses for the reference and after SO_2 exposure at 0.2 A cm^{-2} is mainly due to an increased activation overpotential in the range of 5–15 and 20–30 mV, respectively. An increase in the operating current during SO_2 poisoning resulted in the addition of mass transfer losses to the existing activation overpotential. For example, the observed performance drop for the total cell of 70–80 mV after SO_2 contamination at 0.8 A cm^{-2} (Fig. 6 a) is accounted for by 40–50 mV of activation and 30–40 mV of mass transfer losses. Interestingly, for this particular case, we found that the mass transfer losses increased for segments 9 and 10 and continued to grow with current. Thus, the contribution of activation and mass transfer overpotentials to the spatial performance strongly depended on the location of the segment and eventually led to non-uniform degradation. The observed increase in activation overpotential could be explained by the decreased ECSA, whereas the mass transport limitation likely arose from modification of the electrode structure under SO_2 exposure, presumably due to zero-valent sulfur deposition on the catalyst layer as well as on the cathode microporous layer (MPL) and GDL.

3.3. XPS analysis of the cathode electrode and GDL after SO_2 exposure

The surface composition of a fresh sample, reference and sample exposed to SO_2 at 0.8 A cm^{-2} was studied using high-resolution XPS. Three segments (1, 5 and 10) from the reference and poisoned MEAs were analyzed. We focused not only on the cathode catalyst and GDL but also on the catalyst and GDL from the anodic side. Fig. 7 and Tables 2 and 3 present the average values from the three MEA segments. The surface sulfur (S 2p) content for both reference electrodes was found to be ~0.58 at.%, while the poisoned sample showed a statistically significant increase in the sulfur concentration with 0.80 and 0.96 at.% detected at the anode and cathode, respectively (Fig. 7a) and b) and Table 2).

The Pt surface concentration (Pt 4f) decreased for the poisoned anode and cathode compared to that of the reference sample (Fig. 7a) and b) and Table 2). Additionally, the exposed cathode showed a slightly greater degree of Pt reduction compared to that of the reference cathode (Fig. 7 c), Table 3), which was supported by the larger particle size of the catalyst and ECSA data. High-resolution Pt 4f spectra acquired from segment 1 are presented in Fig. 8 a) and c). The poisoned cathode showed a decrease in the surface concentration of F 1s and an increase in the surface concentration of O 1s, which could indicate depletion and degradation of the fluorinated backbone of the surface ionomer due to the presence of H_2O_2 and free radicals such as $^{\cdot}OH$ and $^{\cdot}OOH$. The increase in fluoride emission during SO_2 exposure was demonstrated by collecting and analyzing effluent water from the cathode outlet [67], which supported our XPS results. We could conclude that degradation of the ionomer and oxidation of the carbon support of MEA under SO_2 exposure resulted in the coarsening of the Pt particles and the ECSA loss.

Interestingly, the exposed cathodic GDL has a significantly higher sulfur concentration on the surface than that of the reference cathodic GDL (1.0 at% vs 0.04 at.% in Fig. 7 d) and Table 2). Fig. 7 d) and f) show that an increase in the surface sulfur concentration in the exposed cathodic GDL is accompanied by an increase in the amount of O 1s, suggesting the formation of SO_x species at the GDL. A comparison of the anodic GDLs for the reference and the exposed MEAs also revealed a slight increase in S content for the exposed sample. XPS results clearly showed that the exposure of the cathode to SO_2 resulted in the formation of S-containing species on both the cathode catalyst surface and GDL. XPS data also provided valuable information on the chemistry of the sulfur species adsorbed on Pt [30,42,52] (Fig. 8 b, d). Typically, two doublet (S $2p_{1/3}$ and S $2p_{2/3}$) peaks are observed in the S 2p region with binding energies of 168.2 and 169.7 eV for low- and high-valent sulfur species such as SO_3^{2-} (sulfite) and SO_4^{2-} (sulfate), respectively. Exposure to SO_2 caused a shift of the S 2p spectra to a lower binding energy due to the reduction of sulfur-containing species. A significant increase in the intensity of the S 2p peaks indicates the additional formation of S-containing species on the Pt surface originating from the air stream. At the same time, small detectable peaks at 163–264 eV assigned to elemental sulfur were observed for the exposed cathode (Fig. 8 c) [30,42,52]. The overall analysis of the samples demonstrates that the surface concentration of the reduced sulfur species was almost two times higher for the poisoned MEA compared to that of the reference (Fig. 7 e). The XPS studies showed the formation of reduced sulfur species and elemental sulfur on the cathode after exposure to SO_2 and completely supported our CV results (Fig. 4, Table 1).

3.4. SO_2 effects on low-Pt PEMFC performance and durability

The obtained results on the performance of low-Pt PEMFCs under exposure to SO_2 were in good agreement with our previous data on the behavior of high-loaded fuel cells under SO_2 contamination, and the reduction of Pt content did not change the mechanism of the SO_2 transformations [53]. However, we found that the performance of low-Pt PEMFCs was more sensitive and less resistant to SO_2 due to a reduced initial performance and potential-dependent SO_2 electrochemistry.

Our results and published literature suggest that at the beginning of poisoning, SO_2 adsorbs on the Pt surface, forming several types of Pt–SO_2 binding structures [68-70], which causes a decrease in the available ECSA required for oxygen reduction [30] and a cell voltage loss (Fig. 2). The adsorbed SO_2 species can be reduced to zero-valent sulfur at a low potential of 0.05–0.5 V [30,41,42,44–46,50] or oxidized to sulfate/bisulfates (SO_4^{2-}/HSO_4^-) at high potential (>0.8 V) [41–46,48,49]. The oxidation state of sulfur at intermediate potentials (0.5–0.8 V) is demonstrated by a mixture of elemental sulfur and SO_x species [31,41,42,68].

The operation of the low-Pt fuel cell at the studied current densities of 0.2–1.0 A cm^{-2} resulted in an initial voltage of 0.6–0.75 V (Fig. 2). SO_2 adsorption at this potential range led to the formation of partially reduced SO_x species and zero-valent sulfur, as shown previously [31,41,42]. These S-containing species continued blocking the Pt surface and shifted the 4-electron ORR pathway to a less efficient 2-electron mechanism. Typically, oxygen reduction requires adsorption and dissociation of the O_2 molecule in a bridge configuration between two Pt sites, but at high SO_x coverage, there are few adjacent sites available. This allows O_2 adsorption to predominantly occur "atop" the Pt atom and led to H_2O_2 formation as an intermediate for the 2-electron ORR. All of these caused a constant decrease in cell voltage, which eventually reached values where the electrochemical reduction of SO_x to S^0 proceeded (0.59–0.49 V). The recorded current-voltage profiles showed an inflection point and drastic local current redistribution at these potentials, which together with the EIS low-frequency inductance indicated an additional electrochemical process occurring in parallel to the ORR (Figs. 2 and 3). Moreover, in our work, the formation of reduced SO_x species and elemental sulfur was determined by XPS and CV methods, which strongly supported the proposed SO_2 transformation pathway under normal operating fuel cell conditions. The observed deviation in the potential of the inflection point at various operating currents might be attributed to increased water production at the cathode at high current, which can scavenge SO_2 and alter the potential of the electroreduction. The cell voltage reached a plateau of 0.510 and 0.295 V with a continuous SO_2 injection into the air stream at 0.2 and 0.8 A cm^{-2}, respectively, whereas operation at 1.0 A cm^{-2} resulted in a cell voltage drop below 0.1 V (Fig. 2).

A comparison of the behavior of high- and low-Pt PEMFCs at 0.2 A cm^{-2} and under SO_2 exposure showed that the voltage drop was 60 and 240 mV, respectively. The performance loss at 1.0 A cm^{-2} reached 0.295 and 0.5 V for high- and low-Pt MEAs, accordingly [53]. Moreover, low-Pt MEAs demonstrated a significant decrease in cathode ECSA after SO_2 poisoning at a low current density with a value of 28.7% compared to 18.2% for a high-Pt MEA (Table 1 and [53]). An increase in the operating current during SO_2 cathode contamination led to an ECSA drop of 37–45.2% for the low-Pt sample, while the high-Pt PEMFC showed only 21.9% ECSA loss. The overall performance decline for low-Pt PEMFC was detected in the range of 70–100 mV, while high-Pt MEA performance decreased by 25–50 mV. Additionally, we compared the parameters of the reference tests for high- and low-Pt PEMFCs. It was found that the cathode ECSA loss for the high-Pt reference MEA was 12%, whereas for low-Pt ECSA drop equaled 16.2% after a constant current hold with pure air. The performance drop for both reference tests was insignificant and averaged between 5 and 15 mV. Therefore, the presence of SO_2 in the air stream resulted in an accelerated degradation of the PEMFCs; in particular, SO_2 affected the degradation of low-Pt fuel cells to a greater extent than that of high-Pt PEMFCs.

Interestingly, similar effects were reported recently on studies investigating a cathode loading impact on MEA degradation induced by voltage cycling [5] and PEMFC stack performance [6]. Ref. [5] showed a strong ECSA loss for low-Pt cathode MEAs compared to that of high-Pt samples under accelerated stress tests. The authors attributed the observations to the different aging behavior of Pt with different sizes and

degrees of agglomeration, although the reasons for the fast degradation of low-Pt MEAs were still not clear. Our results suggest that the observed substantial ECSA and performance loss for low-Pt PEMFC could be explained by accelerated Pt dissolution and redeposition (Ostwald ripening) as well as particle agglomeration in the presence of SO_2. Apparently, the role of SO_2 in these processes was not direct and instead were mediated by the SO_2 impact on the ORR; since the contaminant switched the ORR mechanism from the 4-electron to a mixture of the 4- and 2-electron pathways with the production of H_2O_2 [30–32], which was the main source of free radicals that were the contributors to the ionomer degradation and further agglomeration of Pt particles. Pt dissolution could occur not only at high potentials but also at intermediate potentials (~0.65 V) [71], so we could expect that the released Pt ions at the cathode diffuse toward a membrane, where they are reduced by permeating H_2 from the anode; thus, resulting in the formation of electrically disconnected Pt particles within the membrane [72]. It should be noted that Pt bands in the membrane were detected after PEMFC poisoning by SO_2 [67], which supported the Oswald ripening mechanism for Pt surface area loss. Taking into account the fact that low-Pt MEAs have less catalytic material than high-Pt electrodes, any reduction in available Pt and its surface area through either Pt redeposition in the membrane or as particle agglomeration caused a more drastic effect on the ECSA and performance compared to the high-Pt cathodes. Our results and understanding of SO_2 electrochemical behavior at fuel cell operating conditions suggest that a recovery procedure should include an increase in a cathode potential greater than 1.1 V to oxidize the deposited elemental sulfur species at 35 °C. These potentials cannot be achieved at regular fuel cell operation with air (ocv ~0.95 V) or even with O_2 (ocv ~1.1 V). However, an increase in operating temperature could reduce oxidation potential of S^0 as it is known for carbon monoxide. So, purging cathode with pure O_2 at elevated temperature could be a possible and relatively simple way to recover fuel cell performance. Other rehabilitation approaches involve cathode purging with O_3 (E^0 2.07 V), or electrochemical cycling that is coupled with repeated flushing with pure air. While, these strategies might remove sulfur-containing species from catalyst surface, they cannot undo the damage of irreversible losses arising from the cathode ECSA decline. Furthermore, such recovery procedures deviate from the PEMFC stack standard operating routine and can be performed by specialists at service centers which creates a significant drawback to their commercial viability.

4. Conclusion

In this work, we studied the effects of SO_2 poisoning on the spatial performance of low-Pt PEMFCs at different operating currents using a segmented cell approach. A reduction in cathode Pt loading to 0.1 mg_{Pt} cm^{-2} and its exposure to 2 ppm SO_2 led to 1) a voltage loss below 0.1 V for a fuel cell under exposure of SO_2 operating at a high current; 2) a decrease in the cathode ECSA of up to 45.2%; and 3) a decline in the overall performance after recovery in the range of 70–80 mV with a local performance drop of ~100 mV. Physico-chemical evolution of the poisoned PEMFCs showed that the observed behavior can be attributed to SO_2 electrochemical reduction causing the formation of elemental S^0 on the Pt surface and altering the ORR pathway to a combination of 2- and 4-electron mechanisms with peroxide production. The peroxide production additionally contributes to catalyst degradation, causing ECSA loss that negatively affects fuel cell performance and consequently its durability. The deposition of S^0 on the catalyst surface explained the lack of full self-recovery and necessity of voltage cycling to high potential (>1.2 V) to ensure sulfur oxidation and removal. Moreover, due to formation of elemental sulfur at lower cathode potential, an increase in operating current will promote poisoning effects of SO_2 on low-Pt PEMFCs. All of these findings demonstrate premature degradation of low-Pt PEMFCs in the presence of SO_2 and, from a larger perspective, indicate that the durability, performance and life span of low-Pt fuel cells can be easily compromised during long-term operation under harsh environmental conditions. Since low-Pt PEMFC performance and durability are seriously affected by SO_2 and operations with pure air could not ensure full recovery, it is suggested that SO_2 should be eliminated from air stream.

Declaration of competing interest

The authors declare that they have no known competing financial interests or personal relationships that could have appeared to influence the work reported in this paper.

CRediT authorship contribution statement

Tatyana Reshetenko: Conceptualization, Investigation, Writing - original draft, Writing - review & editing. **Vincent Laue:** Investigation, Writing - original draft. **Ulrike Krewer:** Investigation, Writing - original draft. **Kateryna Artyushkova:** Investigation, Writing - original draft.

Acknowledgements

T. Reshetenko acknowledges financial support from the US Office of Naval Research (N00014-18-1-2127, N00014-19-1-2159). The authors are deeply grateful to T. Carvalho for assistance with TEM, G. Randolf and J. Huizingh for help in segment cell system operation as well as the Hawaiian Electric Company for ongoing support of the Hawaii Sustainable Energy Research Facility.

References

[1] A. Kongkanand, M. Mathias, J. Phys. Chem. Lett. 7 (2016) 1127.
[2] T. Yoshida, K. Kojima, Electrochem. Soc. Interface 24 (2015) 45.
[3] S. Arisetty, X. Wang, R.K. Ahluwalia, R. Mukundan, R. Borup, J. Davey, D. Langlois, F. Gambini, O. Polevaya, S. Blanchet, J. Electrochem. Soc. 159 (2012) B455.
[4] R.K. Ahluwalia, S. Arisetty, J.-K. Peng, R. Subbaraman, X. Wang, N. Kariuki, D. J. Myers, R. Mukundan, R. Borup, O. Polevaya, J. Electrochem. Soc. 161 (2014) F291.
[5] G.S. Harzer, J.N. Schwammlein, A.M. Damjanović, S. Ghosh, H.A. Gasteiger, J. Electrochem. Soc. 165 (2018) F3118.
[6] P. Gazdzicki, J. Mitzel, A.M. Dreizler, M. Schulze, K.A. Friedrich, Fuel Cell. 18 (2018) 270.
[7] J.M. Moore, P.L. Adcock, J.B. Lakeman, G.O. Mepsted, J. Power Sources 85 (2000) 254.
[8] J. St-Pierre, Y. Zhai, M. Angelo, J. Electrochem. Soc. 161 (2014) F280.
[9] A. Talke, U. Misz, G. Konrad, A. Heinzel, D. Klemp, R. Wegener, J. Power Sources 400 (2018) 556.
[10] T.V. Reshetenko, J. St-Pierre, J. Power Sources 287 (2015) 401.
[11] T.V. Reshetenko, J. St-Pierre, J. Power Sources 293 (2015) 929.
[12] T.V. Reshetenko, J. St-Pierre, J. Power Sources 333 (2016) 237.
[13] T.V. Reshetenko, J. St-Pierre, J. Power Sources 378 (2018) 216.
[14] T.V. Reshetenko, K. Artyushkova, J. St-Pierre, J. Power Sources 342 (2017) 135.
[15] J. St-Pierre, M. Virji, J. Appl. Electrochem. 46 (2016) 169.
[16] M. Bétournay, G. Bonnell, E. Edwardson, D. Paktunc, A. Kaufman, A.T. Lomma, J. Power Sources 134 (2004) 80.
[17] P. Faber, F. Drewnick, J. Piske, T. Kurz, S. Borrmann, Int. J. Hydrogen Energy 37 (2012) 17203.
[18] X.-Z. Yuan, H. Li, Y. Yu, M. Jiang, W. Qian, S. Zhang, H. Wang, S. Wessel, T.T. H. Cheng, Int. J. Hydrogen Energy 37 (2012) 12464.
[19] A.A. Franco, B. Barthe, L. Rouillon, O. Lemaire, ECS Trans 25 (2009) 1595.
[20] Y.-G. Yoon, I. Choi, C.-H. Lee, J. Han, H.-J. Kim, E.-A. Cho, S.J. Yoo, S.W. Nam, T.-H. Lim, J.J. Yoon, S. Park, J.H. Jang, Bull. Kor. Chem. Soc. 35 (2014) 3475.
[21] A. Talke, U. Misz, G. Konrad, A. Heinzel, J. Electrochem. Soc. 165 (2018) F3111.
[22] K.-C. Lum, S.-L. Ng, W.-C. Hui, P.-K. Chan, Environ. Monit. Assess. 111 (2005) 55.
[23] Annual summary – Hawaii Air quality data. https://health.hawaii.gov/cab/files/2016/12/aqbook_2015.pdf, 2015.
[24] A.J. Sutton, T. Elias, R. Navarrete, Volcanic gas emissions and their impact on ambient air character at Kilauea Volcano, Hawaii, Open-File Report 94-569. https://digital.library.unt.edu/ark:/67531/metadc707134/, 1994.
[25] M.S. Angelo, J. St-Pierre, ECS Trans 64 (2014) 773.
[26] D. Imamura, E. Yamaguchi, ECS Trans 25 (2009) 813.
[27] Y. Nagahara, S. Sugawara, K. Shinohara, J. Power Sources 182 (2008) 422.
[28] R. Mohtadi, W.-K. Lee, J.W. Van Zee, J. Power Sources 138 (2004) 216.
[29] F. Jing, M. Hou, W. Shi, J. Fu, H. Yu, P. Ming, B. Yi, J. Power Sources 166 (2007) 172.
[30] Y. Garsany, O.A. Baturina, K.E. Swider-Lyons, J. Electrochem. Soc. 154 (2007) B670.

[31] O.A. Baturina, K.E. Swider-Lyons, J. Electrochem. Soc. 156 (2009) B1423.
[32] O.A. Baturina, B.D. Gould, Y. Garsany, K.E. Swider-Lyons, Electrochim. Acta 55 (2010) 6676.
[33] B.D. Gould, G. Bender, K. Bethune, S. Dorn, O.A. Baturina, R. Rocheleau, K. E. Swider-Lyons, J. Electrochem. Soc. 157 (2010) B1569.
[34] J. Fu, M. Hou, C. Du, Z. Shao, B. Yi, J. Power Sources 187 (2009) 32.
[35] P. Jayaraj, P. Karthika, N. Rajalakshmi, K.S. Dhathathreyan, Int. J. Hydrogen Energy 39 (2014) 12045.
[36] S. Tsushima, K. Kaneko, S. Hirai, ECS Trans 33 (2010) 1645.
[37] S. Tsushima, K. Kaneko, H. Morioka, S. Harai, J. Therm. Sci. Technol. 7 (2012) 619.
[38] J.A. Prithi, B.S. Viswanath, N. Rajalakshmi, K.S. Dhathathreyan, Fuel Cell. 17 (2017) 308.
[39] M.M. Saleh, M.I. Awad, F. Kitamura, T. Ohsaka, Int. J. Electrochem. Sci. 7 (2012) 12004.
[40] Y. Zhai, G. Bender, S. Dorn, R. Rocheleau, J. Elcetochem. Soc. 157 (2010) B20.
[41] O. Baturina, B.D. Gould, A. Korovina, Y. Garsany, R. Stroman, P.A. Northrup, Langmuir 27 (2011) 14930.
[42] D. Imamura, ECS Trans 16 (2008) 807.
[43] T. Loučka, Electroanal. Chem. Interfacial Electrochem. 31 (1971) 319.
[44] A.Q. Contractor, H. Lal, J. Electroanal. Chem. 93 (1978) 99.
[45] A.Q. Contractor, H. Lal, J. Electroanal. Chem. 96 (1979) 175.
[46] C. Quijada, A. Rodes, J.L. Vázquez, J.M. Pérez, A. Aldaz, J. Electroanal. Chem. 394 (1995) 217.
[47] C. Quijada, A. Rodes, J.L. Vázquez, J.M. Pérez, A. Aldaz, J. Electroanal. Chem. 398 (1995) 105.
[48] J.A. O'Brien, J.T. Hinkley, S.W. Donne, J. Electrochem. Soc. 157 (2010) F9111.
[49] A.J. Appleby, B. Pichon, J. Electroanal. Chem. 95 (1979) 59.
[50] C. Korzeniewski, W. McKenna, S. Pons, J. Electroanal. Chem. 235 (1987) 361.
[51] M.J. Foral, S.H. Langer, J. Electroanal. Chem. 246 (1988) 193.
[52] K.E. Swider, D.R. Rolison, J. Electrochem. Soc. 143 (1996) 813.
[53] T. Reshetenko, V. Laue, U. Krewer, K. Artyushkova, J. Power Sources 438 (2019) 226949.
[54] US DOE MYRD&D Plan. https://energy.gov/sites/prod/files/2017/05/f34/fcto_myrdd_fuel_cells.pdf.
[55] T.V. Reshetenko, G. Bender, K. Bethune, R. Rocheleau, Electrochim. Acta 56 (2011) 8700.
[56] T.R. Ralph, M.P. Hogarth, Platin. Met. Rev. 46 (2002) 3.
[57] T.E. Springer, T.A. Zawodzinski, M.S. Wilson, S. Gottesfeld, J. Electrochem. Soc. 143 (1996) 587.
[58] C.A. Schiller, F. Ritcher, E. Güzlow, N. Wagener, Phys. Chem. Chem. Phys. 3 (2001) 374.
[59] T.V. Reshetenko, K. Bethune, M.A. Rubio, R. Rocheleau, J. Power Sources 269 (2014) 344.
[60] R.D. Harington, M. Henderson, J. Electroanal. Chem. 39 (1972) 81.
[61] D.A. Harrington, B.E. Conway, Electrochim. Acta 32 (1987) 1703.
[62] Ch-N. Cao, Electrochim. Acta 35 (1990) 831.
[63] J.-P. Diard, B. Le Gorrec, C. Montella, J. Electroanal. Chem. 326 (1992) 13.
[64] P. Córdoba-Torres, M. Keddam, R.P. Nogueira, Electrochim. Acta 54 (2008) 518.
[65] N. Wagner, M. Schulze, Electrochim. Acta 48 (2003) 3899.
[66] S. Thomas, Y.-E. Sung, H.S. Kim, A. Wieckowski, J. Phys. Chem. 100 (1996) 11726.
[67] S. Dorn, Y. Zhai, R. Rocheleau, ECS Trans 28 (2010) 183.
[68] I.R. Moraes, M. Weber, F.C. Nart, Electrochim. Acta 42 (1997) 617.
[69] Y.-M. Sun, D. Sloan, D.J. Alberas, M. Kovar, Z.-J. Sun, J.M. White, Surf. Sci. 319 (1994) 34.
[70] X. Lin, K.C. Hass, W.F. Schneider, B.L. Trout, J. Phys. Chem. B 106 (2002) 12575.
[71] V. Komanicky, K.C. Chang, A. Menzel, N.M. Markovic, H. You, X. Wang, D. Myers, J. Electrochem. Soc. 153 (2006) B446.
[72] P.J. Ferreira, G.J. la O, Y. Shao-Horn, D. Morgan, R. Makharia, S. Kocha, H. A. Gasteiger, J. Electrochem. Soc. 152 (2005) A2256.